Journal of Coastal Research	40	1	31–50	Charlotte, North Carolina	January 2024

Seasonal Morphodynamics of Fringing Reef Pocket Beaches and Responses to Rapid Vertical Tectonic Movements

Sarah Charroux[†‡§]*, Matthieu Jeanson[†‡], Sophie Morisseau[‡††], and Gwenaelle Pennober[†§]

[†]University of Montpellier, IRD,
University of Antilles, University of Guyane
University Réunion
Montpellier, France

[‡]CUFR de Mayotte
Dembéni, Mayotte, France

[§]University of La Reunion
Saint Denis, France

[††]MARBEC (MARine Biodiversity, Exploitation and Conservation)
Université de Montpellier
Montpellier, France

www.cerf-jcr.org

www.JCRonline.org

ABSTRACT

Charroux, S.; Jeanson, M.; Morisseau, S., and Pennober, G., 2024. Seasonal morphodynamics of fringing reef pocket beaches and responses to rapid vertical tectonic movements. *Journal of Coastal Research,* 40(1), 31–50. Charlotte (North Carolina), ISSN 0749-0208.

Determining the morphological response of coastal environments to a general rise in sea level constitutes one of this century's greatest challenges. In 2018–19, Mayotte, a coral reef–fringed island in the Indian Ocean, underwent a volcanic crisis that resulted in island subsidence of up to 0.2 m. This seismo-volcanic crisis made the island an ideal workshop site to observe the response of pocket beaches to sea-level variations. Morphodynamic analyses were carried out on three beaches located on different sides of the island on a biannual basis between 2019 and 2022. Analysis of these survey data showed that the alternation between monsoon and trade winds led to a seasonal rotation of the beaches. Furthermore, the central profiles did not appear to be affected by seasonal variations. As result, they were used to characterize subsidence-related impacts. When the pre- and postsubsidence profiles were compared, morphological changes were not noticeable. However, the rise in the sea level caused by subsidence led to an increase in the frequency of spring flooding at high tide in certain areas of low-lying beaches and roads on the densely populated NE coast of the archipelago, the area most affected by this tectonic movement.

ADDITIONAL INDEX WORDS: *Subsidence, beach mobility, coral reef, 2018–21 Comoro Islands seismic crisis, sea-level rise, coastal flooding.*

INTRODUCTION

Sea-level rise is one of the major challenges identified by the Intergovernmental Panel on Climate Change (IPCC) Special Report (IPCC, 2022). By the end of the 21st century, global mean sea levels are projected to be between +0.43 m (RCP2.6) and +0.84 m (RCP8.5) relative to the period 1986–2005 (IPCC, 2022). The rising sea level could lead to change in cycles of erosion and accretion on beaches. An effect of a higher sea may be increased backshore erosion because the high-energy waves that strip sediment will reach further inshore. Changes in beach morphologies and shoreline migration are expected (IPCC, 2022).

Mayotte Island, in the Mozambique channel (East Africa), was subject to a very rapid tectonic vertical sea-level change from May 2018 to December 2020. In just 2 years, Mayotte experienced a relative sea-level rise of nearly 0.2 m, representing half of the most optimistic sea-level rise scenario by 2100 (+0.43 m) (Cesca *et al*., 2020; Feuillet *et al*., 2019). This crisis therefore makes Mayotte an exceptional site in which to observe the response of beaches to a rapid sea-level rise.

This study focused on the morphological responses of the pocket beaches. Pocket beaches refers to short (about 100 m to a few kilometers long), more or less embayed beaches. These beach compartmentalizations are common along rocky coasts. They are characterized by indented geometries imposed by geological constraints or structures, which, in interaction with waves, can result in beach rotation (Bertin *et al*., 2022). Therefore, pocket beaches can be considered as largely closed systems, without sediment bypass (Dehouck, Dupuis, and Sénéchal, 2009). While large numbers of studies have focused on pocket beaches along open coastlines (Dubois, Sedrati, and Menier, 2011; Horta *et al*., 2018; Vousdoukas *et al*., 2009), only a few have focused on understanding the morphodynamics of coastlines fringed by reefs (Jeanson *et al*., 2013; Norcross, Fletcher, and Merri, 2002; Risandi *et al*., 2020).

The main objective of this study was to observe the potential morphological impacts of a rapid rise in sea level on pocket beaches bordered by fringing reefs. In the context of pocket beaches, seasonal variations need to be understood and differentiated in order to observe medium- and long-term variations. This is why this study began by defining and characterizing the hydrosedimentary variations at the sites studied. Once this had been done, the long-term morphogenic dynamics were studied.

DOI: 10.2112/JCOASTRES-D-23-00021.1 received 23 March 2023; accepted in revision 21 July 2023; corrected proofs received 12 September 2023; published pre-print online 27 October 2023.
*Corresponding author: sarah.charroux@univ-mayotte.fr

Fringing reef beaches are governed by the same general physical mechanisms as other coastal environments, where wave breaking causes wave-induced currents (Monismith *et al.*, 2013). However, in addition to these general mechanisms, fringing reef beaches have complex bathymetry, with steep slopes and high bottom roughness, which can alter shoreline hydrodynamics. The geometric complexity of coral reefs, such as the width of a reef flat or the presence of a back depression or a lagoon, has an impact on hydrodynamic conditions (Brander, Kench, and Hart, 2004; Hearn, 2011; Lowe *et al.*, 2009a; Monismith, 2007; Pomeroy *et al.*, 2012). Reef morphology and shallow water dissipate wave energy through bottom friction. Hydrodynamic conditions depend on the depth of immersion above the reef. A higher water level above the reef will result in less dissipation, and therefore more energy will reach the shore (Lowe *et al.*, 2009b). In meso- to macrotidal contexts, the tide plays an important role. Energy dissipation will be greater at low tide than at high tide (Costa *et al.*, 2016). In reef environments, currents and wave regimes are closely linked and interact in complex ways (Perry *et al.*, 2013). Ocean currents influence the wave regime by moving water horizontally. In addition, strong currents can modify the height, period, and direction of waves by altering the distribution of energy in the ocean. Waves can also be refracted, diffracted, or scattered by currents, altering their direction and behavior.

In addition to climate-related factors, other (so-called static) effects related to Earth's viscoelastic response also produce regional variations in sea level (Kemp *et al.*, 2015). These include tectonic deformation, subsidence, changes in the lithosphere, and human activity.

Tectonic deformation in geodynamically active areas (volcanism, seismicity) is the main cause of static variations in sea level. These are characterized by the sinking or uplifting of the coastal zone (on a decimeter or meter scale). The vertical response to these earthquakes depends on the distance between the coast and the earthquake, the impact of which can reach 300 to 600 km. This deformation, synchronous with the earthquake, may or may not be followed by a phase of postseismic deformation, which may last for years or decades, during which vertical movements of Earth's surface occur (Dura *et al.*, 2016; Shirzaei *et al.*, 2021). These events linked to tectonic changes (uplift or subsidence) are considered to be an important cause of relative sea-level rise, both on large geological scales (Quaternary, Holocene) and short geological scales (last century) (Rovere, Stocchi, and Vacchi, 2016).

At the scale of a volcano or volcanic chain, subsidence can be influenced by various factors such as cooling of the lithosphere, deflation of a magma reservoir, and flexure of the lithosphere linked to volcanic loads (Gargani, 2022; Huppert, Royden, and Perron, 2015). The average rate of subsidence of volcanic islands is 0.01 to 0.1 mm yr^{-1} (Kench, 2015).

The response of the lithosphere to melting ice, also known as glacio-isostatic adjustment, is also an important cause of relative sea-level change. The current rate of glacial-isostatic adjustment is estimated to be around $+10$ mm yr^{-1} in former glacial regions and around -1 to -2 mm yr^{-1} in former periglacial regions (Lidberg *et al.*, 2010). To a lesser extent, isostatic response can also occur when large quantities of sediment are redistributed along the coast (Dalca *et al.*, 2013). The implications of this isostatic response have a major impact on relative variations in sea level on very long timescales (millennia and more) and in areas of high sediment mobility (Dalca *et al.*, 2013).

Finally, certain human activities can cause subsidence (Nicholls and Cazenave, 2010). These include the extraction of fluids from aquifers or hydrocarbon reservoirs (Shirzaei *et al.*, 2021). While these factors are already well known, new ones are beginning to be researched. This is the case for coastal urban development and, more specifically, the concentration of weight in relatively small areas (Parsons, 2021; Wu, Wei, and D'Hondt, 2022).

The causes of sea-level change are numerous, and it can occur temporarily or permanently. In the current context of climate change, it seems essential to understand the response of beaches to sea-level rise. Many studies have focused on the impact of sea-level rise on reefs, but only a few have looked at how fringing reef pocket beaches might respond (Jeanson *et al.*, 2021; Saunders *et al.*, 2016; Webster *et al.*, 2009).

The very rapid subsidence ($+0.05$ to 0.095 m yr^{-1}) of Mayotte makes it an excellent workshop site. Thus, this study aimed to understand the current morphodynamics of Mayotte's pocket beaches and whether they have been modified by this rapid sea-level rise. For this purpose, a study of the hydrodynamic conditions in the trade wind and monsoon seasons was carried out and combined with analyses of morphological variations. Then, a comparison was made with the old topographic surveys to examine potential differences.

METHODS

This study focused on measuring seasonal variations in marine weather conditions (wind and wave climate) and their impact on the morphology of pocket beaches (topographical changes). Then, the behavior of the beaches was compared to previous topographic data obtained from Mayotte beaches to observe changes that could be linked to the very rapid tectonics movements. All survey dates and instruments are summarized in Tables 1–3. First, the geological and climatic context of the study site will be described, followed by a presentation of the methods used to monitor seasonal variations in morphodynamics.

Table 1. *Topographic survey dates.*

Season	Mtsamboro	Sakouli	Ngouja
Monsoon 2018			20 Apr 2018
Monsoon 2019			11 Apr 2019
Dry 2019	30 Sep 2019	3 Sep 2019	
Monsoon 2020	11 Mar 2020	8 Apr 2020	24 Apr 2020
Dry 2020	18 Sep 2020	19 Oct 2020	20 Oct 2020
Monsoon 2021	1 Apr 2021	31 Mar 2021	12 Apr 2021
Dry 2021	10 Sep 2021	19 Oct 2021	20 Oct 2021
Monsoon 2022	3 Mar 2022	22 Mar 2022	31 Mar 2022
Dry 2022	27 Sep 2022	28 Oct 2022	28 Sep 2022

Table 2. *Hydrodynamic survey dates.*

Season	Location	Instrument	Coordinates	Start of Measurements	End of Measurements
Monsoon	Mtsamboro	Pressure sensor	12°41′45.02″ S, 45°03′52.83″ E 12°41′50.40″ S, 45°04′0.95″ E	1 Mar 2021	15 Mar 2021
	Sakouli	ADCP	12°53′21.34″ S, 45°12′54.81″ E	21 Jan 2022	10 Feb 2022
		Pressure sensor	12°53′22.62″ S, 45°12′55.59″ E 12°53′18.54″ S, 45°12′50.90″ E		
	Ngouja	ADCP	12°57′50.81″ S, 45°05′08.99″ E	14 Jan 2022	2 Mar 2022
		Pressure sensor	12°57′54.10″ S, 45°05′07.69″ E 12°57′48.82″ S, 45°05′10.84″ E		
Dry	Mtsamboro	Pressure sensor	12°41′45.02″ S, 45°03′52.83″ E 12°41′50.40″ S, 45°04′0.95″ E	9 Sep 2021	23 Sep 2021
	Sakouli	ADCP	12°53′21.34″ S, 45°12′54.81″ E	17 May 2021	2 Jun 2021
		Pressure sensor	12°53′22.62″ S, 45°12′55.59″ E 12°53′18.54″ S, 45°12′50.90″ E		
	Ngouja	ADCP	12°57′50.81″ S, 45°05′08.99″ E	10 Jun 2022	29 Jun 2022
		Pressure sensor	12°57′54.10″ S, 45°05′07.69″ E 12°57′48.82″ S, 45°05′10.84″ E		

Study Area

Located in the Southern Hemisphere, Mayotte forms the Comoros archipelago along with the islands of Anjouan, Mohéli, and Grande Comore. This archipelago lies to the north of the Mozambique Channel, between Madagascar and the southern part of the African continent. It is the result of a geological event dating from around 180 Ma, when the vast continent of Gondwana, which then included Africa, Madagascar, India, Australia, and Antarctica, began to gradually fragment, creating the Comoros Basin (Michon, 2016; Tzevahirtzian *et al*., 2020). The Comoros archipelago represents the emerged peaks of the Davie ridge. The phenomena at the origin of this volcanic rift are still difficult to establish with certainty. Two main theories have been put forward to explain the formation of the archipelago. They differ mainly in the origin of the magmatism. The volcanism of the archipelago could be associated with the presence of a hot spot at depth (Debeuf, 2004; Hajash and Armstrong, 1972), or it could be linked to regional lithospheric fractures induced by interactions between the Somali plate and the Lwandle block in a context of extension created by the detachment of Madagascar (Lemoine *et al*., 2020; Tzevahirtzian *et al*., 2020; Upton, 1982).

Whatever its origin, the volcanic activity that formed the Comoros archipelago began around 20 Ma with the formation of the island of Mayotte (Michon, 2016). This formation can be separated into four main stages: (1) between 20 and 1.95 Ma, with the formation of the southern shield volcano, (2) between 8 and 0.8 Ma, when volcanic activity led to the creation of the northern shield volcano, (3) between 2.7 and 0.15 Ma, when the northwestern complex was formed, and finally (4) between 0.15 Ma and 4000 YBP, when Petite Terre was formed. The current relief of Mayotte is the result of 20 million years of construction, erosion, and alteration (Debeuf, 2004; Vittecoq *et al*., 2014).

Covering an area of 374 km^2, Mayotte (12°50′ S, 45°10′ E) is made up of two main islands: Grande Terre and Petite Terre, as well as around 30 volcanic or coral islands. The island's geological history and environmental context have resulted in the development of a barrier reef of around 160 km^2, interspersed with numerous passes, enclosing a vast lagoon of 1500 km^2 and an almost continuous fringing reef.

Volcanic activity on the island had been relatively calm for 4000 years, but since May 2018, the volcano-tectonic situation on the island of Mayotte has undergone a new event without precedent on a historical scale. Significant seismic

Table 3. *Shoreline retreat dates for Sakouli.*

Instrument	Date
Digitalized	18 Oct 2008
Total station	3 Sep 2019
Digitalized	2 Nov 2020
Total station	8 May 2021

activity has affected the island, with 1109 events of magnitude >3.5 recorded between May and November 2018 (Lemoine *et al*., 2020). This seismic activity is the result of the deflation of a magma reservoir located at a depth of around 30 km beneath Petite Terre, leading to the creation of a new submarine volcanic edifice around 50 km east of Petite-Terre. This edifice is named Fani Maoré, and it is 800 m high and located at a depth of 3500 m (Cesca *et al*., 2020; Feuillet *et al*., 2019). The earthquakes associated with this volcanic activity formed two swarms with epicenters grouped together at sea: between 5 and 15 km east of Petite Terre for the proximal swarm and 25 km east of Petite Terre for the distal swarm, at depths mostly between 25 and 50 km (Cesca *et al*., 2020; Feuillet *et al*., 2019). The majority of these earthquakes were of low magnitude, although several light- to moderate-magnitude earthquakes were recorded (the maximum occurring on 15 May 2018 with a magnitude of 5.9). Although the number of earthquakes has decreased since 2018, seismicity continues, with 360 earthquakes recorded in February 2023 (REVOSIMA, 2023). This volcanic activity moved the island eastwards by 21 to 25 cm and vertically (subsidence) by 10 to 19 cm (REVOSIMA, 2023).

Climate of the Study Area

Due to its location, Mayotte has a humid tropical climate, with a rainy monsoon season from November to March (austral summer) and a dry trade wind season from May to September (austral winter) separated by transition periods. During the monsoon season, the wind blows from the N to S with a moderate intensity (mean speed of 3.3 m s^{-1}), while during the trade wind season, the wind blows from the S to N with a stronger intensity (mean speed of 5.1 m s^{-1}) (Météo-France, 2022). Even though Mayotte is relatively sheltered by Madagascar, maximum wind speeds occur when tropical storms or cyclones pass offshore in the Mozambique channel between December and April. Previous studies in the Mayotte reef flat and lagoon (Jeanson *et al*., 2013) showed that the offshore wave climate of Mayotte is closely related to the seasonal wind regime. Austral summer winds generate moderate waves from the NW to NE, while sustained and regular trade winds generate waves from the S to SE (60%). Around 50% of waves are below 2 m in height, while heights above 2 m account for 8% to 15% of cases (Jeanson *et al*., 2013). This study showed that the wave climate of Mayotte is dominated by moderate waves with characteristic periods of 5 to 6 s, which correspond to regional fetch. Tides are semidiurnal, and the tidal range is mesotidal, with a mean spring range of about 3.2 m.

Description of Beaches

To study beach evolution due to seasonal variations and the potential effects of subsidence, three different sites were chosen for the variety of their morphology, sediment grain sizes, and wave exposures. Mtsamboro is located on the northwest coast (12°41′53″ S, 45°04′09″ E), Sakouli is on the center east (12°53′18″ S, 45°12′43″ E), and Ngouja is on the southwest (12°57′44″ S, 45°04′47″ E) (Figure 1). To characterize study sites, a rapid analysis of beach grain size was carried out. Mtsamboro is the most urbanized site (Figure 2), with the village directly behind the beach, and a wall defining the shoreline. The beach is 500 m long and 30 m wide, with a median grain size (D_{50}) of 229 μm and around 52% bioclastic material. This beach is the outlet for two small streams, in which solid flows are monitored as part of a project to combat silting up of the lagoon. For information, the watershed area considered is 19 ha and showed an average erosion rate of 4.11 t ha^{-1} y^{-1} between 2015 and 2019, with significant annual disparities. Indeed, as the 2017–18 rainy season was very wet, the average erosion rate for that year was 6.81 t ha^{-1}, whereas in other years, erosion rates ranged from 3.78 to 2.90 t ha^{-1} (Desprats *et al*., 2018, 2019). Sakouli (Figure 3) and Ngouja (Figure 4) are less anthropized beaches. Their rear beaches are mainly vegetation with only a few backwater resorts. However, they are not located on the same coast, so their exposure to wind and waves is different. Sakouli is oriented to the SE, while Ngouja is oriented SW. Furthermore, Ngouja grain size is coarser than Sakouli sand (D_{50} = 484 μm and D_{50} = 184 μm, respectively). The Ngouja beach is composed of nearly 70% of bioclastic material, while Sakouli is composed of only 35% (Table 4). This may correspond to differences in wave exposures. There are no permanent watercourses in the Sakouli watershed area, only temporary runoff during heavy rainfall from two gullies (in the center and the south parts of the beach) that empty onto the beach. Like Sakouli, the Ngouja watershed has no perennial watercourse, so most of the land sediment input is runoff.

Marine Weather Conditions

To study hydrodynamic forcing, trihourly wind data (speed and direction) were collected by the meteorological station of Pamandzi (12°48′00″ S, 45°16′48″ E), operated by the French meteorological service (Météo-France). Local wind data allow differentiation between swells coming from the open sea, wind sea waves, and waves generated in the lagoon.

The aim of the hydrodynamic experiments was to characterize differences in wave conditions between two normal forcing mechanisms. Hydrodynamic field experiments were performed for around 20 days during the 2021–22 monsoon and trade wind seasons at Sakouli (21 January 2022–10 February 2022; 17 May 2021–2 June 2021, respectively) and Ngouja (14 February 2022–2 March 2022; 10 June 2022–29 June 2022, respectively) beaches. These periods correspond to classic wind and wave monsoon and trade wind periods. Wave and current measurements were recorded with an acoustic Doppler current profiler (ADCP; Nortek Signature 1000) deployed in bottom-mounted frames. Data were obtained at a frequency of 2 Hz in bursts of 15 minutes every 30 minutes. The sensor was located 70 cm above the seabed on a steel tripod, on a sandy area in the middle of the reef flat (12°32′58″ S, 45°04′00″ E in Sakouli and 12°57′51″ S, 45°05′08″ E in Ngouja). Due to field work difficulties (theft and damage of equipment), Mtsamboro was only instrumented with pressure sensors (RBR solo 3D) to obtain wave parameters such as significant height (H_s), peak period (T_p), and water level. Pressure sensor data were recorded at 2 Hz. Once

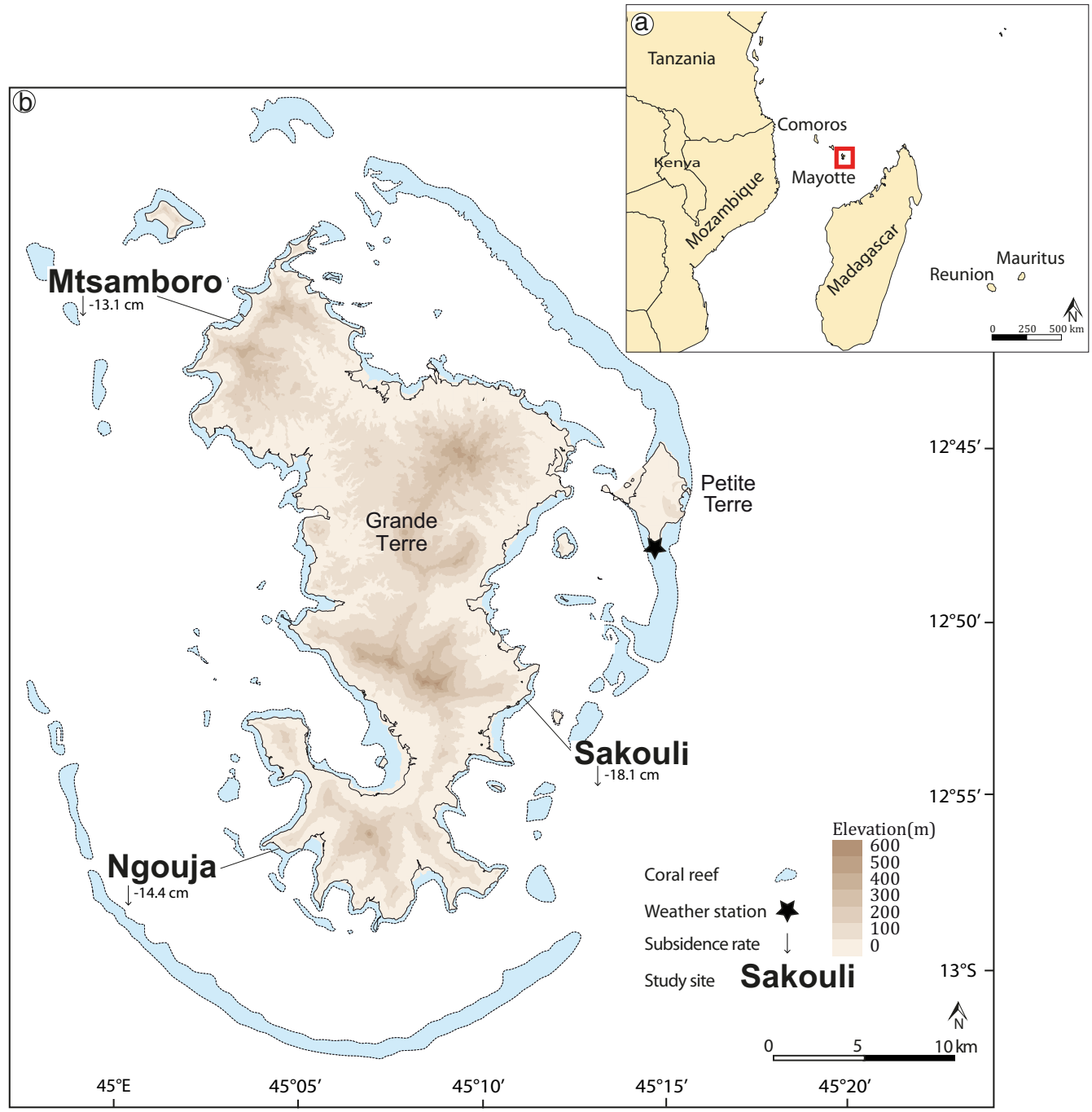

Figure 1. Location of Mayotte island in the Indian Ocean (a) and (b) study sites.

data were Fourier transformed, the wave spectrum was obtained. In order to ensure data quality, samples with an amplitude peak (high or low) were deleted. In the same way, samples with ADCP beam correlations of <50% were deleted. Finally, to avoid electronic noise, all values acquired in <1 m of water were suppressed.

Current profilers use an internal compass, which allowed orientation of the data from magnetic north. In Mayotte, magnetic declination is not negligible, being around 8°. Therefore, the data were corrected for the magnetic declination and set up in relation to the geographic north.

Figure 2. Location of the three profiles at the Mtsamboro study site (white lines) (base map: orthophotography from IGN, public domain).

Beach Morphological Change

To observe seasonal topographic variations, biannual cross-shore beach profiles were made using a real-time kinematic global navigation satellite system (GNSS-RTK). Then, series of orthorectified aerial photographs from 2008 and 2020 were used to assess long-term temporal variations in the shoreline position and rates of change.

Cross-Shore Profile Evolution

Cross-shore beach profiles were measured on the three beaches in each season, beginning in September 2019 (during spring tide) using the GNSS-RTK system (Trimble RS8 TSC3) with errors within ±3 cm. The official coordinate system of Mayotte (RGM04) was used for the measurement in easting and northing (Universal Transverse Mercator Zone 38S) and elevation (datum SHOM 1953). All surveys were carried out on foot at low tide, with the profile lines extending from a benchmark at the top of the beach until a depth of at least −1 m. On each beach, three profiles were consistently monitored (P100, south; P200, center; P300, north). These profiles were compared to older profiles (2008 and 2018) when these were available (Jeanson *et al.*, 2019, 2021). On pocket beaches, the seasonal changes in wind and wave patterns lead to a beach rotation, which means a transition of the sediment from one part of the beach to another in response to the hydrodynamic regime. This rotation of the beaches induces more marked movements on the ends of the beaches (P100, P300). The central profile (P200) does not seem to be affected by permanent sedimentation. Thus, to see the multiyear variations in beach morphology and the potential impact of rising water, the central profiles (P200) of the beaches were compared to old profiles surveyed in 2008.

The rapid subsidence that affected Mayotte has led to a modification of the island's benchmarks. Georeferencing work will need to be carried out in the coming years by the French National Institute of Geographic and Forest Information (IGN-F) and the French Hydrographic and Oceanographic Service (SHOM), but this has not yet been done because the stabilization of vertical movements is still recent. Consequently, the profiles for 2019 to 2021 were adjusted to take into account the following subsidence values (Grandin

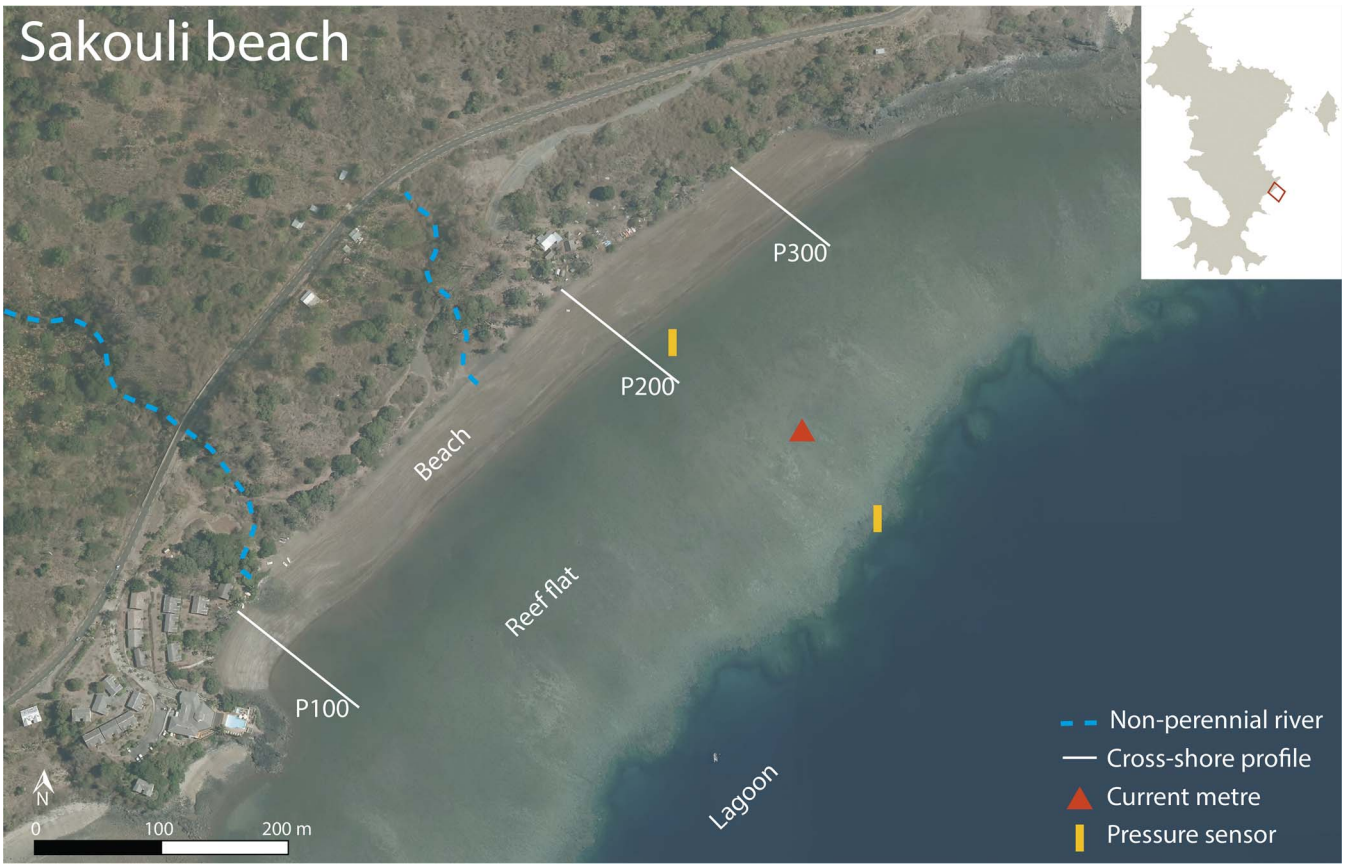

Figure 3. Location of the three profiles (white lines), the current meter (red triangle), and pressure sensors (yellow rectangle) at the Sakouli study site (base map: orthophotography from IGN, public domain).

et al., 2019): 13.1 cm for Mtsamboro (the least subsident part of Mayotte), 18.1 cm for Sakouli (on the most subsident eastern part), and 14.4 cm for Ngouja.

The total beach volumetric change for each transect (in cubic meters per unit meter beach length) was computed by integrating the beach profile upward from the mean low water neap (MLWN) level (Cohen, 2014).

Shoreline Evolution

To characterize shoreline evolution, remote and *in situ* methods were used on Sakouli beach. Ngouja beach was not surveyed due to the size of the vegetation canopy in the upper beach, which did not allow a clear definition of the shoreline. The seawall at the top of the beach on Mtsamboro made it inconsistent to characterize the shoreline evolution of this site. Based on orthorectified and georeferenced photographs of Sakouli beach from the IGN-F in 2008 and 2020, the shoreline was screen digitized at a scale of 1:1000 in QGIS 3.16.7 software along the coast. The pixel size of the 2008 image was 0.5 m, while it was 0.2 m in the 2020 image. The shoreline was defined as the limit of the vegetation, as in previous studies (Ford, Becker, and Merrifield, 2013; Kench and Brander, 2006a; Yates *et al.*, 2013). In areas with large canopies, the vegetation limit does not represent the coastline, so these areas were removed from consideration to reduce uncertainty.

The total error of uncertainty on the shoreline position (U_{tot}) was 2.1 m for 2018 and 2 m for 2020. This error was obtained using Equation (1) of Hapke *et al.* (2011):

$$U_{tot} = \sqrt{U_{geo}^2 + U_{res}^2 + U_{tra}^2} \quad (1)$$

where, U_{geo} is the georeferencing error (U_{geo} = 0 m), U_{res} is the spatial resolution of the photograph (U_{res} = 0.5 m in 2008 and 0.2 m in 2020), and U_{tra} is the uncertainty from shoreline tracing accuracies (estimated to be 2 m for each date, because of the scale used during the tracing process). To minimize errors, the top of the beach was also extracted from the topographic profile of the beach center.

The *in situ* coastline was plotted using a total station (Nikon XF). The top of the microcliff was measured at each major topographic change in 2019 and 2021. The total station was chosen for coastline monitoring because of the presence of trees with a large canopy at the top of the beach, which prevented the DGPS-RTK from picking up enough satellites to achieve good resolution. All survey dates are summarized in Tables 1–3.

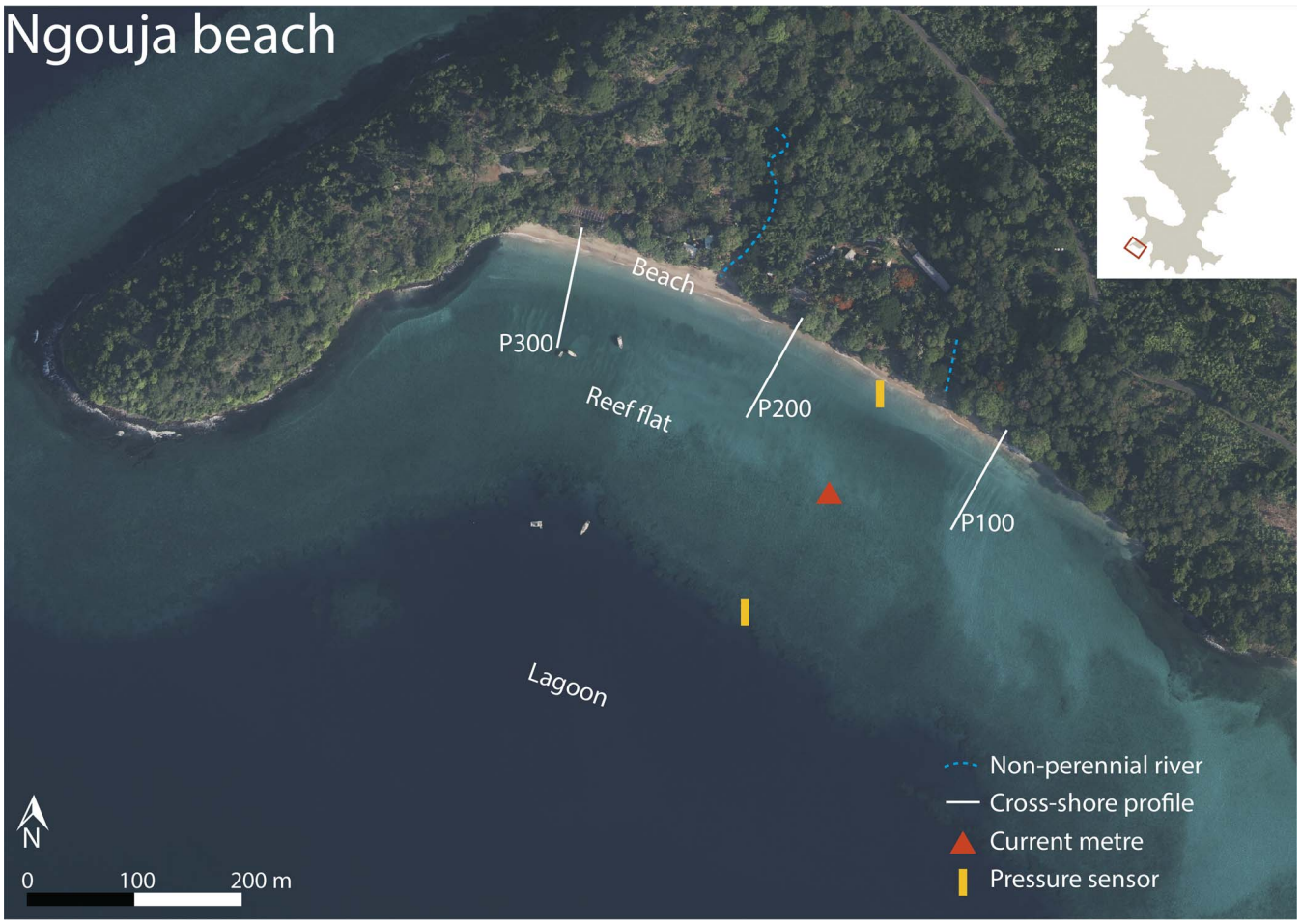

Figure 4. Location of the three profiles (white lines), the current meter (red triangle), and pressure sensors (yellow rectangle) at the Ngouja study site (base map: orthophotography from IGN, public domain).

RESULTS

These field acquisitions made it possible to obtain information in terms of forcing and impact on both seasonal and subsidence scales. Thus, the study outcomes are presented in three sections. First the forcing conditions and then their impacts on seasonal beach morphology are shown. Finally, the multiyear morphological changes are discussed.

Forcing Conditions

The wind conditions for the two seasons of 2020 and 2021 are summarized in Figure 5. The meteorological data for the years monitored after subsidence are in line with average climate trends for the region (1951–2007) (Jeanson, 2009). There was a marked difference in wind intensity and direction between the trade wind season and the monsoon season. During the trade wind season, the winds were predominantly from the south (more than 70% are from the SE to SSW) with a mean of 4.75 m s^{-1}. During this season, about 10% of the average trihourly winds were faster than 8 m s^{-1} and could even reach 12.8 m s^{-1}. In the monsoon season, however, the winds had lower intensities, with a mean of 3.18 m s^{-1}, and only 2% were faster than 8 m s^{-1}. During the monsoon season, the winds were more variable in direction with about 30% to the NW.

Table 4. *Beach morphodynamic parameters.*

	Mtsamboro	Sakouli	Ngouja
Median grain size (μm)	229	185	484
Percentage of bioclastic material (%)	52	35	70
Beach length (m)	500	600	650
Beach width (m)	30	40	50
Reef flat width (m)	400	220	250
Shoreface slope (tanβ)	0.10	0.05	0.14

The wind conditions measured during the field campaigns confirmed that these campaigns were carried out during the classic forcing conditions of each season. The waves resulting from the action of the wind in Mayotte are special because of the important reef context. In the Sakouli reef flat, the swell direction is mostly SSE (95%) during the dry season, while the swell orientation is more variable during the monsoon

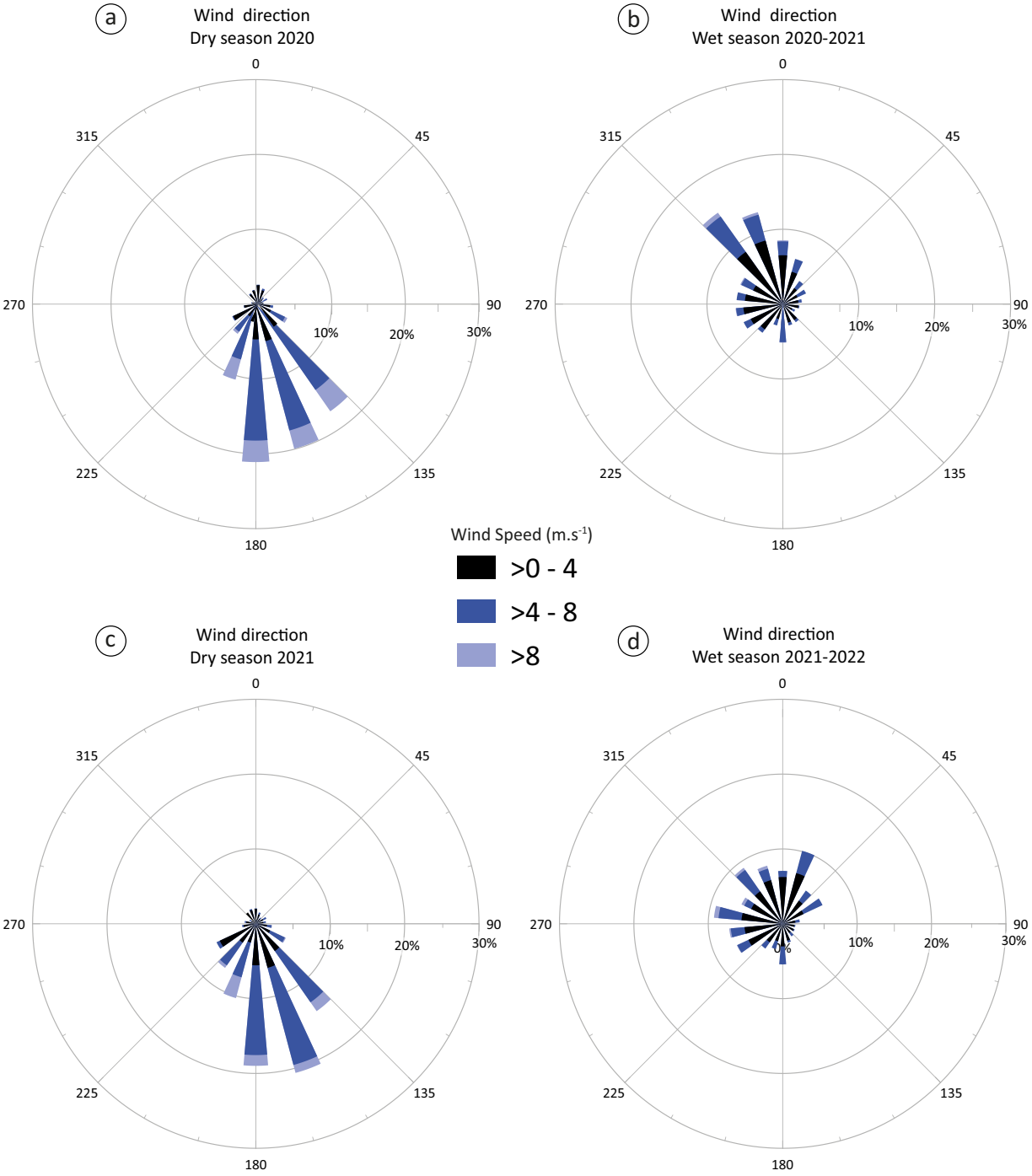

Figure 5. Wind roses for (a) dry (trade wind) season 2020, (b) monsoon season 2020–21, (c) dry season 2021, and (d) monsoon season 2021–22. Data are from Météo-France, public domain.

season. Current directions also experience the same variations. In January (monsoon season), the average current over the measurement period was 0.04 m s^{-1}, with 97% of values lying below 0.1 m s^{-1}, and the orientations were very variable. During this same period, the maximum reached was 0.12 m s^{-1} from the NE. In May (trade wind season), currents were from SSW with a higher intensity (mean of 0.06 m s^{-1}). In this study, 88% of currents were below 0.1 m s^{-1}, and almost 4% were bigger than 0.15 m s^{-1}, reaching up to 0.23 m s^{-1} (Figure 6).

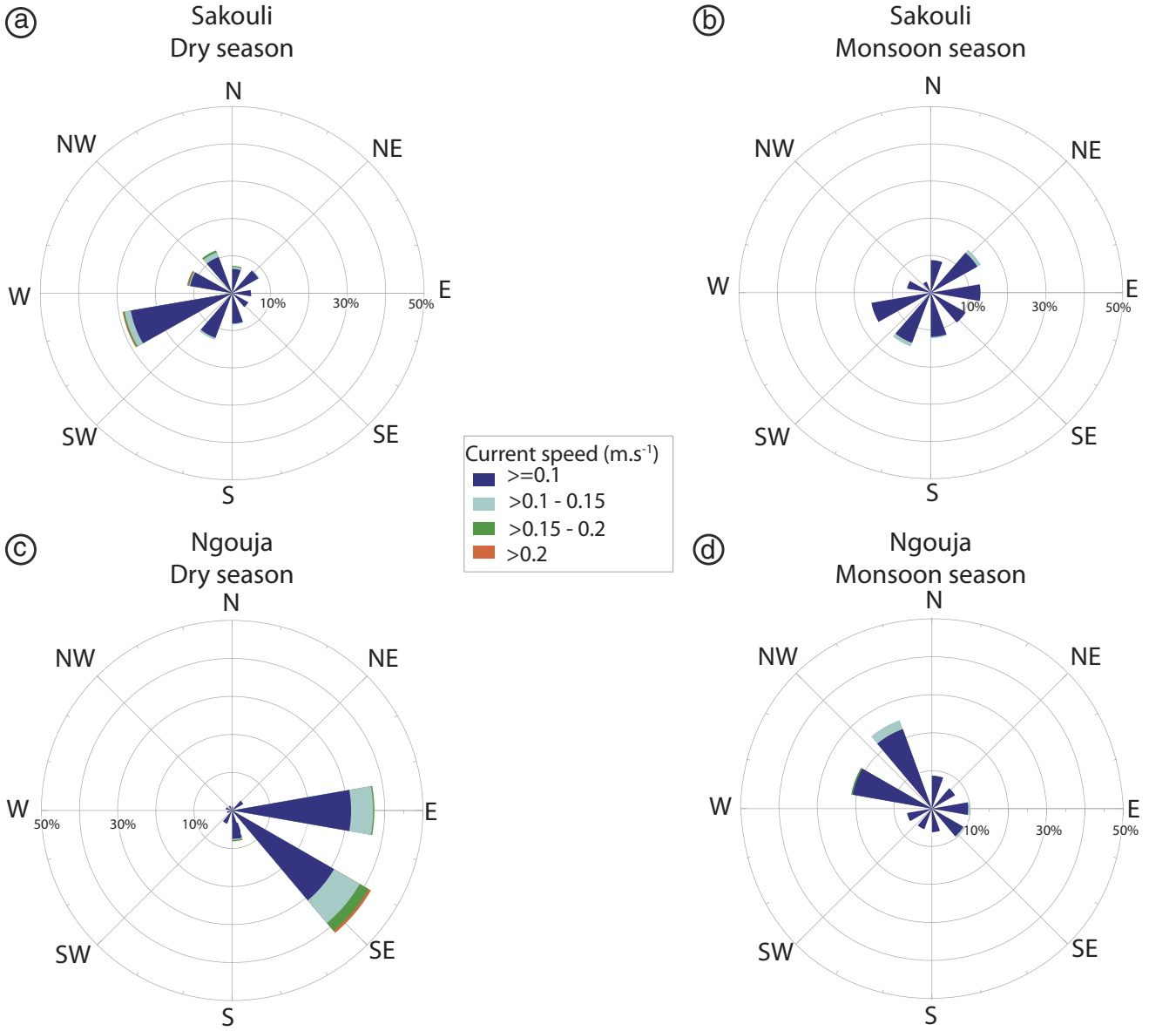

Figure 6. Rose of currents in the dry and wet seasons on the Sakouli (a and b) and Ngouja (c and d) flats. Currents are given according to their origin.

In the Ngouja reef flat, hydrodynamics were also different depending on the season. Swells were mostly SW for both seasons, but they were more variable in the dry season. Currents experienced more contrasted seasonal variations. During the monsoon season (February), most of the current came from the NNW (25%) and WNW (21%). There was a large majority (96%) of current below 0.1 m s^{-1}, and the average current over the measurement period was 0.05 m s^{-1}. In June (trade wind season), currents were stronger, with an average of 0.7 m s^{-1}, and 4% of values were bigger than 0.15 m s^{-1}. During this period, 38% of currents came from E, and 42% came from the SE (Figure 6).

In this highly protected hydrodynamic context, for all the selected beaches, wave heights were higher during the trade wind season than during the monsoon season (Table 5). Waves were higher in Ngouja than in the other beaches, especially during the monsoon season, at 0.3 m and 0.1 m, respectively (Table 5). The survey at Mtsamboro beach in September 2021 recorded 0.3 m and 0.7 m for average and maximum H_s, respectively. In March 2021, the average and maximum H_s values were 0.1 m and 0.4 m, respectively. The Sakouli beach exhibited a similar pattern to Mtsamboro in May 2021, with 0.3 m and 0.7 m as average and maximum H_s, respectively. As for the dry season, in January 2022, Sakouli beach showed

Table 5. *Wave parameters for each beach and in each season.*

	Dry Season			Monsoon Season		
	Mtsamboro	Ngouja	Sakouli	Mtsamboro	Ngouja	Sakouli
H_s (m)						
Mean	0.3	0.4	0.3	0.1	0.3	0.1
Standard deviation	0.1	0.1	0.1	0.1	0.1	0.1
Max	0.7	0.8	0.7	0.4	0.6	0.5
50th percentile	0.2	0.4	0.3	0.1	0.3	0.1
75th percentile	0.4	0.4	0.4	0.1	0.3	0.2
T_p (s)						
Mean	12.3	8.9	6.0	10.5	10.1	7.6
Standard deviation	2.4	3.1	2.4	4.7	3.7	2.9
Max	18.3	20.0	18.4	19.7	17.9	20.0
50th percentile	12.2	7.6	5.4	12.2	10.5	7.9
75th percentile	14.2	11.8	6.6	14.2	12.8	9.2

little differences, with 0.1 m and 0.5 m as average and maximum H_s, respectively. The H_s readings for Ngouja in June and February were higher than those of the two other beaches: 0.4 m and 0.8 m as average and maximum for June, and 0.3 m and 0.6 m as average and maximum for February (Table 5). In addition, wave periods were different for all beaches and both seasons. They were higher during the dry season than the monsoon season for Mtsamboro and Ngouja, at 12.3 seconds and 8.9 seconds, respectively, while Sakouli recorded a higher wave period during the monsoon season than during the dry season at 7.6 seconds and 6.0 seconds, respectively (Table 5).

Seasonal Morphological Changes

First of all, over the study period of 2019–22, the Mtsamboro beach did not present a major seasonal variation (the average of differences between trade wind and monsoon seasons of the beach was 0.05 m for the north part and 0.13 m for the south part) (Figure 7). The north part remained almost stable with a maximum of difference between trade wind and monsoon seasons of 0.12 m. The south part experienced more seasonal variations with a maximum difference of 0.27 m. Sediment budget was similar for most seasons, between -1.6 to $+2.9$ m^3 m^{-1}. However, the 2020–21 monsoon season experienced a gain of 16.7 m^3 m^{-1}, and the 2022 dry season experienced a loss of -24 m^3 m^{-1}. So, for the entire measurement period, there was a loss of -16.3 m^3 m^{-1}, with a majority of gain during the monsoon season and a majority of loss during the dry season (Figure 7c).

In Sakouli, the beach with the highest subsidence rate, there was a change of 0.73 m between the dry and the wet season in the north part (P300) of the beach (Figure 8). However, the south profile (P100) did not show any major variation, with a mean of 0.15 m between the trade wind season and monsoon season. The overall sediment budget of Sakouli beach was almost constant between seasons, with a maximum volume difference between the seasons of $+9$ m^3 m^{-1} for the monsoon season 2019–20 compared to the others (Figure 8c). However, there was a change in sand distribution in the beach, with $+5.81$ m^3 m^{-1} for the north profile during the 2020 trade wind season.

Finally, the Ngouja beach profiles showed major seasonal variation (Figure 9). In the north part (P300), the monsoon season profile was 0.10 m higher than the dry season profile, while the monsoon season was 1.53 m lower than the dry season in the south part (P100). As it is also possible to see in Figure 9c, there was a volume change between seasons and profiles. Usually, during the monsoon season, the north part of the beach lost part of the sand, around 20 m^3 m^{-1}, while the south part gained sediment. These phenomena were reversed during the dry season. However, the 2021–22 monsoon season resulted in a gain of about 20 m^3 m^{-1}, which changed the sediment balance of the beach. This beach rotation was higher than that in other seasons.

Pluriannual Topographic Changes

Figure 10 shows the evolution of the central (P200) cross-shore profile from 2008 to 2022 during the monsoon season. On the beaches of Mtsamboro and Ngouja, no major differences can be observed between the 2008 profiles and the post-subsidence profiles (maximum of differences of 0.07 m and 0.29 m, respectively). However, it is possible to observe variations on the position of the microcliff at Sakouli.

To measure the retreat of this microcliff of Sakouli, the differences between 2008 and 2019–2020–2021 retreat was measured. For this purpose, surveys of the top of the microcliff were carried out using a total station in 2019 and 2021. The 2008 and the 2020 shorelines were digitalized using the limit of vegetation because the cliff top is covered by grass. The retreat between the 2008 and 2019 profiles was about 0.12 m yr^{-1}, while that between 2019 and 2022 increased to 0.48 m yr^{-1} (Figure 11).

DISCUSSION

The study objective was to observe the morphological response of pocket beaches in a context of very rapid subsidence. However, on Mayotte's beaches, the hydrodynamic conditions are mostly determined by the seasonal influence of the wind climate (Jeanson *et al.*, 2013, 2019). Therefore, this work first focused on seasonal variations in beach morphodynamics in order to observe subsidence-related changes.

As shown in Figure 6, the intensity and direction of the currents depend on the season. In the trade wind season, the

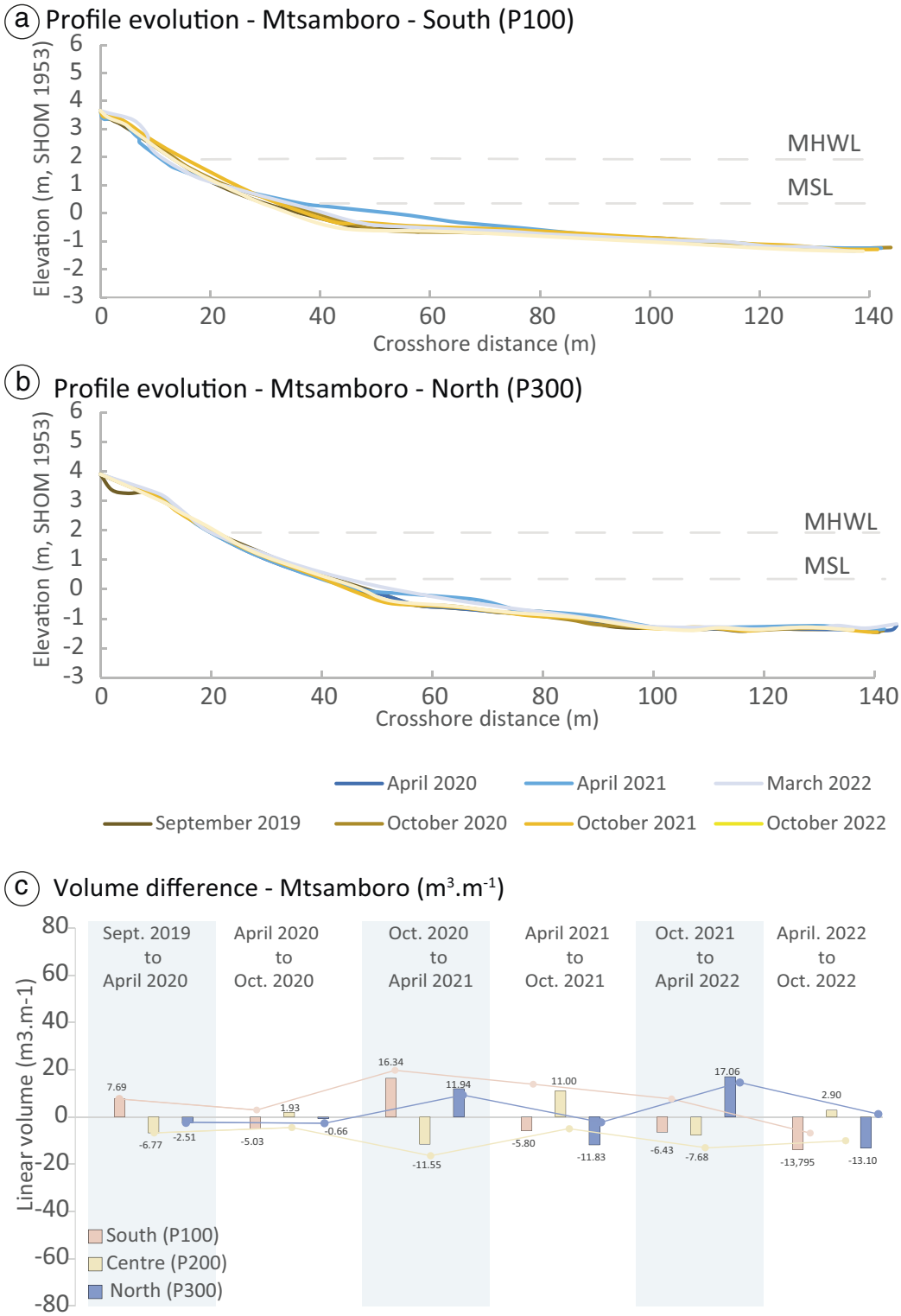

Figure 7. Mtsamboro beach profile: (a) south profile; (b) north profile; and (c) volume differences. MHWL = mean high water level, MSL = mean sea level, MLWL = mean low water level.

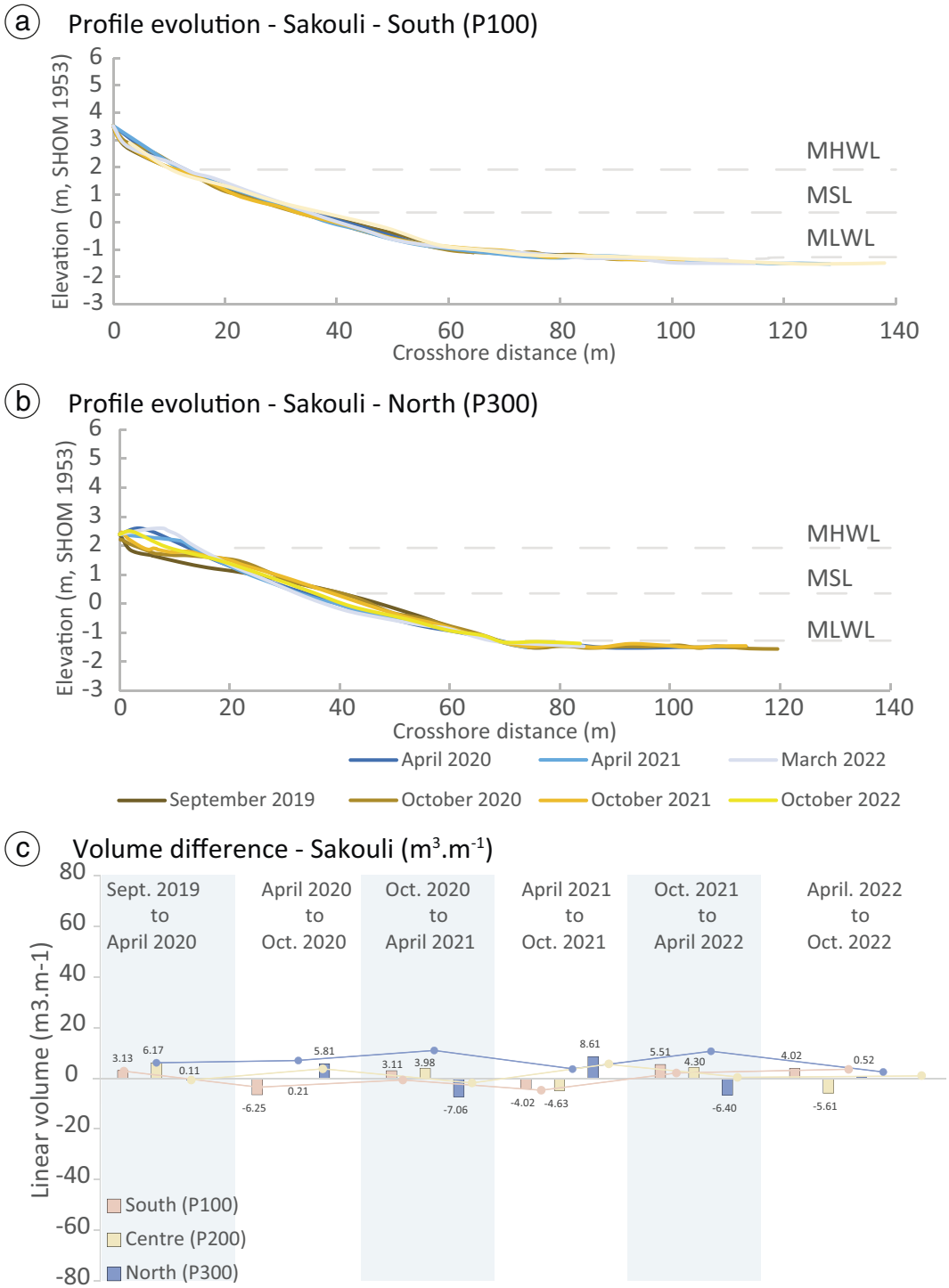

Figure 8. Sakouli beach profile: (a) south profile; (b) north profile; and (c) volume differences from 2019 to 2022. MHWL = mean high water level, MSL = mean sea level, MLWL = mean low water level.

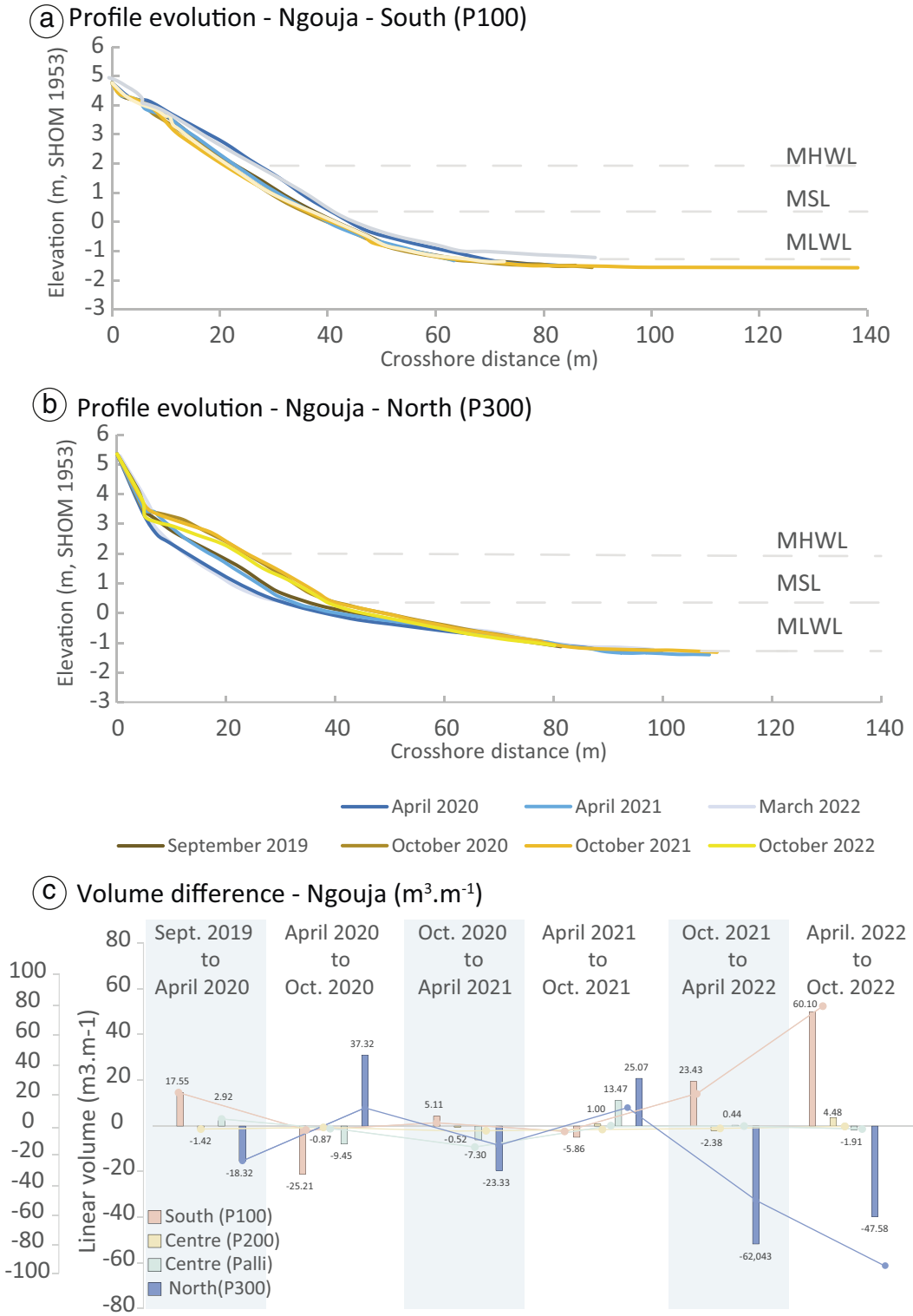

Figure 9. Ngouja beach profile: (a) south profile; (b) north profile; and (c) volume differences. MHWL = mean high water level, MSL = mean sea level, MLWL = mean low water level.

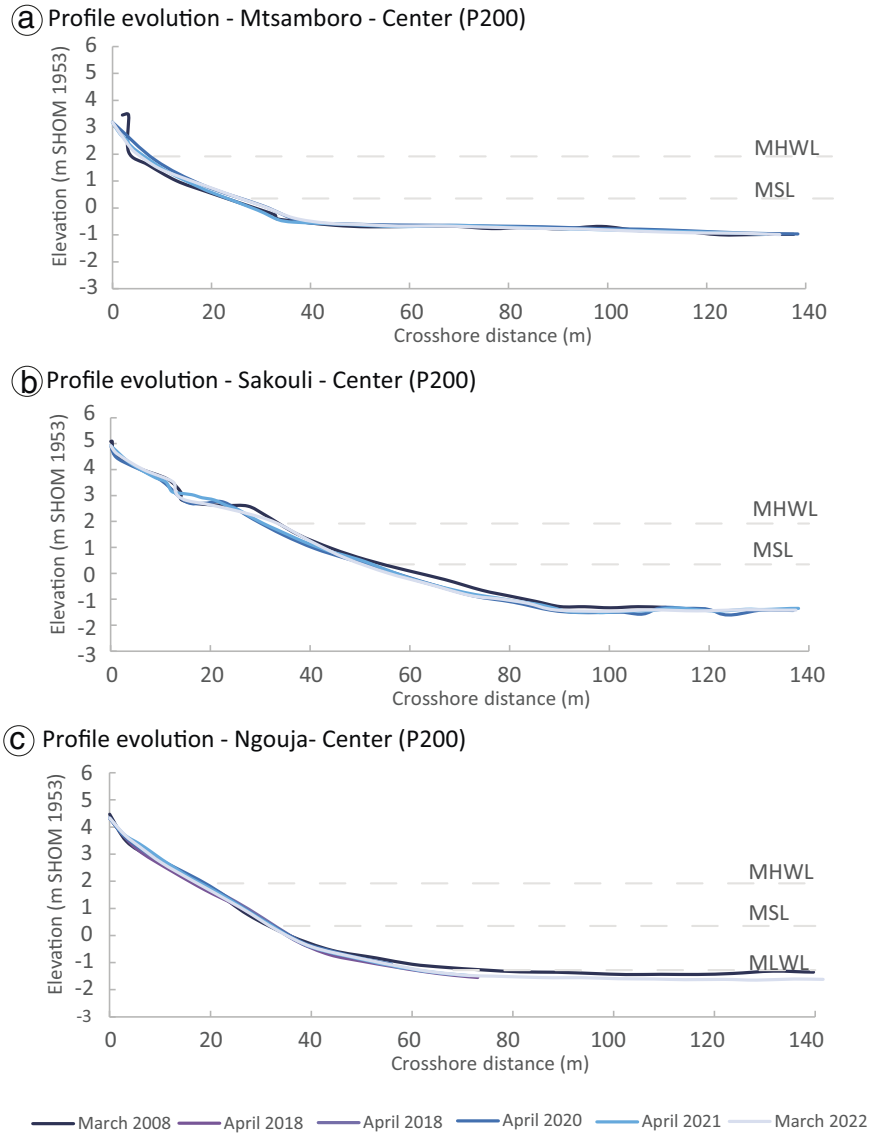

Figure 10. Central profile evolution from 2008 to 2022 in March for (a) Mtsamboro, (b) Ngouja, and (c) Sakouli. MHWL = mean high water level, MSL = mean sea level, MLWL = mean low water level.

currents come mainly from the S, linked to a prevailing southerly wind. Conversely, in the monsoon season at Ngouja (Figure 6), currents come mainly from the NW, linked to prevailing northerly winds. On the Sakouli reef flat (Figure 6), the currents have no preferential orientation in the monsoon season, in response to weak winds with no particularly marked origin. Variations in peak periods can also be associated with seasonal wind variations. During the trade wind season, stronger and more directional winds generate sea waves that propagate over the reef. These waves have shorter periods than the offshore swells. Locally generated waves are not attenuated by the barrier reef. Under normal conditions (absence of low pressure), these waves, unattenuated by the barrier reef, can have greater H_s than the offshore swells.

These major shifts in currents and orientations of waves induce sediment transport over the beach. In Ngouja, there was a clear and marked seasonal variation, with sand accumulation in the north part and sand loss in the south part during the trade wind season. In Mtsamboro, the main changes in the north part were due to a gain of sediment below the mean sea level (MSL) in the monsoon season, probably related to discharge of sediment from a watercourse next to the profile. In the south part during the monsoon season, a watercourse disperses sediments from the top to the bottom of the beach, while during the dry season, higher hydrodynamic activity moves sediment from the bottom to the top of the beach. In Sakouli, this alternation was less visible over the cross-shore profiles. This was probably due to the location of the south

Figure 11. Sakouli shoreline variation from 2008 (blue), 2019 (green), 2020 (orange), and 2021(red). Close-up shows the most important retreat in the center of the beach (base maps: orthophotography from IGN, public domain).

profile (P100). Protected by a natural rocky deposit, there was no measurable morphology change in this profile. However, visible changes were observed in the southern part, where there was sand accumulation during the monsoon season and sand loss during the dry season. It was therefore possible to observe a more or less marked seasonal rotation of the beaches from the north to the south during the monsoon season and from the south to the north during the dry season. This beach rotation had already been observed and described in other beaches of Mayotte (Jeanson *et al*., 2013, 2019). However, despite this sediment transport, the total sand balance of the beaches remained almost identical (Figures 7–9).

The seismic-volcanic crisis in Mayotte has led to very rapid subsidence. This subsidence has altered the water level on the reef flat and consequently the level of water reaching the coast. For the moment, the effects of recent subsidence by +0.2 m on the beach and associated coral platform are not evident when comparing the 2006/2008 topographic profiles with the postseismic profiles (Figure 10). This means that the potential response of beaches to sea-level rise depends on multiple factors in addition to the rate of sea-level change, such as geological context, hydrodynamic conditions, accommodation space, and sediment supply (Cooper *et al*., 2020). For example, after the last postglacial sea-level rise, many contemporary beaches retreated inland, but they still exist and are considered to be wide and healthy beaches (Castelle *et al*., 2018).

Four years after the beginning of subsidence, the monitoring of cross-shore profiles showed no morphological changes associated with this very rapid subsidence. However, in some beaches in Mayotte, visible and measurable signs of erosion are present. In the Sakouli beach, the study of the variability in shoreline position shows a clear retreat. Although not linear over the whole beach in terms of intensity, this retreat is visible along the whole length of the beach, with some areas more marked than others (Figure 11). This result needs to be moderated due to methodology bias (multiple operators, changes of instruments, no data available between 2008 and 2019, no data just before and after the subsidence), possible changes in meteorological conditions (higher energetic conditions at high tide during 2019–22 than 2008–19), and long-term morphological response to hydrodynamic impacts. However, although it must be qualified, there was a visible increase in the retreat of the microcliff, which may be related to the increase of the relative sea level. Indeed, the rate of the microcliff retreat increased by a factor of 4 between the periods 2008–19 and 2019–22

Figure 12. Photographs of (a) a fallen tree in Sakouli and (b) overwash in Ngouja (Charroux, October 2020).

(Figure 11). At Sakouli and Ngouja, signs of erosion (fallen trees) and sand scattering (overwash) are visible (Figure 12). They occur when the wave runup exceeds the top of the beach or when the top of the beach is eroded by prolonged wave impact. Overwash could impact the overall sediment balance of the beach and therefore change its equilibrium.

Although the impact of subsidence is still low over the cross-shore profiles and in most beach shoreline positions, the increase of the water level could lead to different reactions by the reef flat (Neumann and Macintyre, 1985). The influences of sea-level rise in coral reef systems are numerous and mainly depend on the intensity of the rise and the state of health of the reef. Indeed, these ecosystems are highly dependent on temperature and light conditions, so they could grow by taking advantage of the new space available or fail to adapt and therefore end up dying (Neumann and Macintyre, 1985). As reef flats play an important role in wave attenuation (Kench and Brander, 2006b; Lowe *et al*., 2005; Lugo-Fernandez, Roberts, Suhayda, 1998; Samosorn and Woodroffe, 2008; Young, 1989), a modification of their composition could alter the energy arriving on the beaches and thus modify the coastline (Sheppard *et al*., 2005; Storlazzi *et al*., 2011). If there is colonization of a reef flat, more energy should be attenuated, and less will reach the beach, whereas if coral colonies decrease, then there will be more wave energy reaching the beach. This will therefore have an impact on the beach equilibrium.

The important factor in beach equilibrium is the sediment supply. In coral reef–fringed pocket beaches, sediment comes from the inland input from the drainage basin (lateritic and volcanic sands) or from the degradation of bioclastic materials (coral, calcareous algae, mollusc shells). In the medium to long term, and depending on the reaction of the corals, an increase in wave energy on the reef flat could lead to further degradation of the coral and increase the input of bioclastic sediments on the beaches. Furthermore, due to higher sea level during storm conditions, sand present at the toe of the reef crest could be remobilized and transferred to the beach (Masselink, Beetham, and Kench, 2020). However, due to higher wave energy, sediment from the beach may be transported offshore, leading to a loss in the sediment budget and therefore to erosion.

Mtsamboro is the most urbanized beach of this study, with a village of 7705 people directly behind the beach. Ngouja and Sakouli are two beaches with high touristic value. Ngouja is the most emblematic beach of Mayotte, while Sakouli is the most touristic beach of the island. Beach attendance is multiplied by 4.3 between weekdays and holidays, reaching almost 300 people in Ngouja on a Sunday. Although less urbanized, Sakouli and Ngouja remain two beaches with leisure facilities (hotels, diving clubs, *etc*.) at the back of the beach, making them sites with high economic value. A recent study (Courteille *et al*., 2022) characterized the vulnerability of all three beaches from 1950 to 2016 using multiple indices, such as morphodynamic, ecological, and anthropogenic factors. As a result, Mtsamboro appears to be the most vulnerable site, mainly due to ecological and anthropogenic factors. The higher hydrodynamic conditions make Ngouja slightly more vulnerable than Sakouli (Courteille *et al*., 2022). These results were obtained from aerial photographs taken before the subsidence (from 1950 to 2016), which means that they do not take into account the subsidence. The increase in the sea level could impact hydrodynamic conditions, leading to an increase in the morphodynamic vulnerability index. Sakouli and Ngouja are more likely to be affected since they have higher subsidence rates (18.1 cm and 14.4 cm, respectively) (Grandin *et al*., 2019). Mtsamboro, located in the northwest of the island, has undergone sinking of 13.1 cm, but the village is more protected due to the presence of a wall.

To cope with this growing population, many development projects have been launched. Studies of the coastal dynamics as well as the potential impacts of a rise in sea level are therefore essential to best manage these projects.

CONCLUSIONS

This study investigated the morphodynamics of three beaches in Mayotte that may have changed due to seasonal wind and wave variations and recent subsidence of almost 20 cm. Upon comparison, Mtsamboro appears to have been less impacted than Ngouja and Sakouli, which display visible signs of erosion in their upper parts. In both the monsoon and dry seasons, Ngouja experiences higher wave energy compared to Sakouli and Mtsamboro, which have relatively lower wave energy. This difference is particularly pronounced during the monsoon season. As expected, all three beaches present a seasonal beach rotation. This rotation is from the northern part to the southern part of the beach during the dry (trade wind) season and the exact opposite during the monsoon season.

While the seasonal rotation of the beaches is relatively well marked in the profiles located at the extremities, the central profiles do not show any major seasonal variation. Thus, the changes observed in these profiles correspond not to seasonal variations but to longer-term variations. Since the second objective of this study was to observe the potential impact of a rapid rise in sea level on the pocket beaches bordered by fringing reefs, a comparison was made between the central profiles produced after 2018 and those produced before subsidence. This comparison did not show any major variations. However, *in situ* observations revealed signs of erosion and sand transfer to land in some areas of Sakouli and Ngouja, which were not recorded in the topographic profiles. In the longer term, these variations could have an impact on the sediment budget of the beach and lead to a change in morphology.

The complementary nature of these approaches has once again proved to be essential in the study of the phenomena present in Mayotte and the exceptional nature of the rapid subsidence. For the time being, 4 years after the onset of subsidence, the monitoring of cross-shore profiles has not revealed any significant morphological changes that could be unequivocally associated with this rapid subsidence.

Finally, it seems necessary in a coral context to associate the morphological responses of the beaches with the biological and morphological responses of the reefs. It is therefore important to continue these studies and to extend them to the study of coastal ecosystems, for example, by monitoring coral growth.

This study has shown the short-term effects of rapid sea-level rise and needs to be continued and extended to a longer timescale to observe the response of reef beaches to sea-level rise. In addition to the continuation of this work, it seems important to update the benchmarks of Mayotte. Indeed, its benchmarks have been rendered inaccurate due to the sinking and displacement of the island. These corrections should be carried out by the IGN-F and SHOM during a referencing campaign between now and the end of 2023, thus enabling high-resolution monitoring.

ACKNOWLEDGMENTS

The authors would like to thank Yann Mercky for his help during data acquisition in the field. Sarah Charroux benefited from a thesis grant from the University Center of Mayotte and the DEAL of Mayotte. Constructive comments and suggestions were provided by four anonymous reviewers.

LITERATURE CITED

Bertin, S.; Floc'h, F.; Le Dantec, N.; Jaud, M.; Cancouët, R.; Franzetti, M.; Cuq, V.; Prunier, C.; Ammann, J.; Augereau, E.; Lamarche, S.; Belleney, D.; Rouan, M.; David, L.; Deschamps, A.; Delacourt, C., and Suanez, S., 2022. A long-term dataset of topography and nearshore bathymetry at the macrotidal pocket beach of Porsmilin, France. *Scientific Data*, 9(13). doi:10.1038/s41597-022-01170-3

Brander, R.W.; Kench, P.S., and Hart, D., 2004. Spatial and temporal variations in wave characteristics across a reef platform, Warraber Island, Torres Strait, Australia. *Marine Geology*, 207(1–4), 169–184. doi:10.1016/j.margeo.2004.03.014

Castelle, B.; Guillot, B.; Marieu, V.; Chaumillon, E.; Hanquiez, V.; Bujan, S., and Poppeschi, C., 2018. Spatial and temporal patterns of shoreline change of a 280-km high-energy disrupted sandy coast from 1950 to 2014: SW France. *Estuarine, Coastal and Shelf Science*, 200, 212–223. doi:10.1016/j.ecss.2017.11.005

Cesca, S.; Letort, J.; Razafindrakoto, H.N.T.; Heimann, S.; Rivalta, E.; Isken, M.P.; Nikkhoo, M.; Passarelli, L.; Petersen, G.M.; Cotton, F., and Dahm, T., 2020. Drainage of a deep magma reservoir near Mayotte inferred from seismicity and deformation. *Nature Geoscience*, 13(1), 87–93. doi:10.1038/s41561-019-0505-5

Cohen, O., 2014. *Profiler 3.1 XL, un logiciel gratuit pour la construction et l'analyse de profils topographiques dans Microsoft Excel©*. Nantes, France: Centre Francais du Littoral, pp. 557–564. doi:10.5150/jngcgc.2014.061

Cooper, J.A.G.; Masseling, G.; Coco, G.; Short, A.; Castelle, B.; Rogers, K.; Anthony, E.J.; Green, A.N.; Kelley, J.T., and Pilkey, O.H., 2020. Sandy beaches can survive sea-level rise. *Nature Climate Change*, 10(11), 993–995. doi:10.1038/s41558

Costa, M.B.S.F.; Araújo, M.; Araújo, T.C.M., and Siegle, E., 2016. Influence of reef geometry on wave attenuation on a Brazilian coral reef. *Geomorphology*, 253, 318–327. doi:10.1016/j.geomorph.2015.11.001

Courteille, M.; Jeanson, M.; Collin, A.; James, D.; Claverie, T.; Charpentier, M.; Gairin, E.; Trouillefou, M.; Giraud-Renard, E.; Dolique, F., and Lecchini, D., 2022. Characterisation of long-term evolution (1950–2016) and vulnerability of Mayotte's shoreline using aerial photographs and a multidisciplinary vulnerability index. *Regional Studies in Marine Science*, 55, 102537. doi:10.1016/j.rsma.2022.102537

Dalca, A.V.; Ferrier, K.L.; Mitrovica, J.X.; Perron, J.T.; Milne, G.A., and Creveling, J.R., 2013. On postglacial sea level—III. Incorporating sediment redistribution. *Geophysical Journal International*, 194(1), 45–60. doi:10.1093/gji/ggt089

Debeuf, D., 2004. Etude de l'évolution volcano-structurale et magmatique de Mayotte, Archipel des Comores, Océan Indien: Approches structurale, pétrographique, géochimique et géochronologique. Saint-Denis, La Réunion: Université de la Réunion, Ph.D. dissertation, 277p.

Dehouck, A.; Dupuis, H., and Sénéchal, N., 2009. Pocket beach hydrodynamics: The example of four macrotidal beaches, Brittany, France. *Marine Geology*, 266(1–4), 1–17. doi:10.1016/j.margeo.2009.07.008

Desprats, J.; Chowanski, E.; Landemaine, V.C.B.D.G.; Rinaudo, J.; Said, K.; Vignerot, B.; Vitter, M., and Bailby, E., 2018. *Projet LESELAM 2 (Lutte contre l'Erosion des Sols et l'Envasement du LAgon à Mayotte) Rapport Avancement no. 1, Décembre 2018*. Orléans, France: Bureau de Recherches Géologiques et Minières, *BRGM/RP- 68559-FR*, 73p.

Desprats, J.; Landemaine, V.; Said, K.; Bailby, E.; Vignerot, B.; Rinaudo, J.; Vitter, M.; Hamidou, A., and Beudard Vérificateur, F., 2019. *Projet LESELAM 2 (Lutte contre l'Erosion des Sols et l'Envasement du LAgon à Mayotte) Rapport Avancement no. 2, Décembre 2019*. Orléans, France: Bureau de Recherches Géologiques et Minières, *BRGM/RP- 69441 -FR*, 66p.

Dubois, A.; Sedrati, M., and Menier, D., 2011. Morphologic response of four pocket beaches to high energy conditions: Including the Xynthia storm (south Brittany, France). In: Furmańczyk, Giza, A., and Terefenko, P. (eds.), Proceedings of the 11th International

Coastal Symposium ICS2011. *Journal of Coastal Research*, Special Issue No. 64, pp. 1845–1849.

Dura, T.; Engelhart, S.E.; Vacchi, M.; Horton, B.P.; Kopp, R.E.; Peltier, W.R., and Bradley, S., 2016. The role of Holocene relative sea-level change in preserving records of subduction zone earthquakes. *Current Climate Change Report*, 2, 86–100. doi:10.1007/s40641-016-0041-y

Feuillet, N.; Jorry, S.; Crawford, W.; Deplus, C.; Thinon, I.; Jacques, E.; Saurel, J.; Paquet, F.; Satriano, C.; Aiken, C.; Foix, O.; Kowalski, P.; Laurent, A.; Cathalot, C.; Donval, J.; Guyader, V.; Gaillot, A.; Scalabrin, C.; Moreira, M.; Beauducel, F.; Grandin, R.; Ballu, V.; Daniel, R.; Pelleau, P.; Gomez, J.; Geli, L.; Bernard, P.; Bachelery, P.; Fouquet, Y.; Bertil, D.; Lemarchand, A., and der Woerd, V., 2019. Birth of a large volcanic edifice through lithosphere-scale dyking offshore Mayotte (Indian Ocean). *Proceedings of the American Geophysical Union Fall Meeting* (San Francisco, California), abstract V043-01.

Ford, M.R.; Becker, J.M., and Merrifield, M.A., 2013. Reef flat wave processes and excavation pits: Observations and implications for Majuro Atoll, Marshall Islands. *Journal of Coastal Research*, 29(3), 545–554. doi:10.2112/JCOASTRES-D-12-00097.1

Gargani, J., 2022. Isostatic adjustment, vertical motion rate variation and potential detection of past abrupt mass unloading. *Geosciences*, 12(8), 302. doi:10.3390/geosciences12080302

Grandin, R.; Beauducel, F.; Peltier, A.; Ballu, V.; Chanard, K.; Valty, P.; Bonnefond, P.; de Chabalier, J.B.; Shreve, T.; Koudogbo, F.N.; Anne, U.; Filatov, A.; Novali, F.; Durand, P., and Komorowski, J.C., 2019. Surface deformation during the 2018–19 Mayotte seismo-volcanic crisis from GNSS, synthetic aperture radar and seafloor geodesy. *Proceedings of the American Geophysical Union Fall Meeting* (San Francisco, California), abstract V52D-03.

Hajash, A. and Armstrong, R., 1972. Paleomagnetic and radiometric evidence for the age of the Comores Islands, west central Indian Ocean. *Earth and Planetary Science Letters*, 16(2), 231–236.

Hapke, C.J.; Himmelstoss, A.; Kratzmann, M.; List, J., and Thieler, R., 2011. *National Assessment of Shoreline Change: Historical Shoreline Change along the New England and Mid-Atlantic Coasts*. Woods Hole, Massachusetts: U.S. Geological Survey, Woods Hole Coastal and Marine Science Center, *Open-File Report 2010-1118*, 57p.

Hearn, C.J., 2011. Perspectives in coral reef hydrodynamics. *Coral Reefs*, 30(S1), 1–9. doi:10.1007/s00338-011-0752-4

Horta, J.; Oliveira, S.; Moura, D., and Ferreira, Ó., 2018. Nearshore hydrodynamics at pocket beaches with contrasting wave exposure in southern Portugal. *Estuarine, Coastal and Shelf Science*, 204, 40–55. doi:10.1016/j.ecss.2018.02.018

Huppert, K.L.; Royden, L.H., and Perron, J.T., 2015. Dominant influence of volcanic loading on vertical motions of the Hawaiian Islands. *Earth and Planetary Science Letters*, 418, 149–171. doi:10.1016/j.epsl.2015.02.027

IPCC (Intergovernmental Panel on Climate Change), 2022. Sea level rise and implications for low-lying islands, coasts and communities. *In:* IPCC (ed.), *The Ocean and Cryosphere in a Changing Climate: Special Report of the Intergovernmental Panel on Climate Change*. Cambridge: Cambridge University Press, pp. 321–446. doi:10.1017/9781009157964.006

Jeanson, M., 2009. Morphodynamique du littoral de Mayotte—Des processus au réseau de surveillance. Dunkerque, France: Université du Littoral Côte d'Opale, Ph.D. dissertation, 348p.

Jeanson, M.; Anthony, E.J.; Charroux, S.; Aubry, A., and Dolique, F., 2021. Detecting the effects of rapid tectonically induced subsidence on Mayotte Island since 2018 on beach and reef morphology, and implications for coastal vulnerability to marine flooding. *Geo-Marine Letters*, 41(4), 51. doi:10.1007/s00367-021-00725-4

Jeanson, M.; Anthony, E.J.; Dolique, F., and Aubry, A., 2013. Wave characteristics and morphological variations of pocket beaches in a coral reef-lagoon setting, Mayotte Island, Indian Ocean. *Geomorphology*, 182, 190–209. doi:10.1016/j.geomorph.2012.11.013

Jeanson, M.; Dolique, F.; Anthony, E.J., and Aubry, A., 2019. Decadal-scale dynamics and morphological evolution of mangroves and beaches in a reef-lagoon complex, Mayotte Island. *In:* Castelle, B. and Chaumillon, E. (eds.), *Coastal Evolution under Climate Change along the Tropical Overseas and Temperate Metropolitan France*. *Journal of Coastal Research*, Special Issue No. 88, pp. 195–208. doi:10.2112/SI88-015.1

Kemp, A.C.; Hawkes, A.D.; Donnelly, J.P.; Vane, C.H.; Hill, T.D.; Anisfeld, S.C.; Parnell, A.C., and Cahill, N., 2015. Relative sea-level change in Connecticut (USA) during the last 2200 yrs. *Earth and Planetary Science Letters*, 428, 217–229.

Kench, P.S., 2015. Coral reefs. *In:* Masselink, G. and Gehrels, R. (eds.), *Coastal Environments and Global Change*. New York: Wiley, pp. 380–409. doi:10.1002/9781119117261.CH16

Kench, P.S. and Brander, R.W., 2006a. Response of reef island shorelines to seasonal climate oscillations: South Maalhosmadulu atoll, Maldives. *Journal of Geophysical Research*, 111(F1). doi:10.1029/2005JF000323

Kench, P.S. and Brander, R.W., 2006b. Wave processes on coral reef flats: Implications for reef geomorphology using Australian case studies. *Journal of Coastal Research*, 22(1), 209–223.

Lemoine, A.; Briole, P.; Bertil, D.; Roullé, A.; Foumelis, M.; Thinon, I.; Raucoules, D.; de Michele, M.; Valty, P., and Colomer, R.H., 2020. The 2018–2019 seismo-volcanic crisis east of Mayotte, Comoros islands: Seismicity and ground deformation markers of an exceptional submarine eruption. *Geophysical Journal International*, 223(1), 22–44. doi:10.1093/gji/ggaa273

Lidberg, M.; Johansson, J.M.; Scherneck, H.-G.; Milne, G.A., and Eshagh, M., 2010. Recent results based on continuous GPS observations of the GIA process in Fennoscandia from BIFROST. *Journal of Geodynamics*, 50(1), 8–18. doi:10.1016/j.jog.2009.11.010ï

Lowe, R.J.; Falter, J.L.; Bandet, M.D.; Pawlak, G.; Atkinson, M.J.; Monismith, S.G., and Koseff, J.R., 2005. Spectral wave dissipation over a barrier reef. *Journal of Geophysical Research: Oceans*, 110(C4), 1–16. doi:10.1029/2004JC002711

Lowe, R.J.; Falter, J.L.; Monismith, S.G., and Atkinson, M.J., 2009a. A numerical study of circulation in a coastal reef-lagoon system. *Journal of Geophysical Research: Oceans*, 114(C6). doi:10.1029/2008JC005081

Lowe, R.J.; Falter, J.L.; Monismith, S.G., and Atkinson, M.J., 2009b. Wave-driven circulation of a coastal reef-lagoon system. *Journal of Physical Oceanography*, 39(4), 873–893. doi:10.1175/2008JPO3958.1

Lugo-Fernandez, A.; Roberts, H.H., and Suhayda, J.N., 1998. Wave transformations across a Caribbean fringing-barrier coral reef. *Continental Shelf Research*, 18(10), 1099–1124.

Masselink, G.; Beetham, E., and Kench, P.S., 2020. Coral reef islands can accrete vertically in response to sea level rise. *Science Advances*, 6(24), 3656–3666.

Météo-France, 2022. *Les saisons à Mayotte*. https://meteofrance.yt/fr/climat/les-saisons-mayotte

Michon, L., 2016. The volcanism of the Comoros archipelago integrated at a regional scale. *In*: Bachelery, P.; Lenat, J.-F.; Di Muro, A., and Michon, L. (eds.), *Active Volcanoes of the Southwest Indian Ocean: Piton de la Fournaise and Karthala*. Berlin: Springer, pp. 333–344.

Monismith, S.G., 2007. Hydrodynamics of coral reefs. *Annual Review of Fluid Mechanics*, 39, 37–55. doi:10.1146/annurev.fluid.38.050304.092125

Monismith, S.G.; Herdman, L.M.M.; Ahmerkamp, S., and Hench, J.L., 2013. Wave transformation and wave-driven flow across a steep coral reef. *Journal of Physical Oceanography*, 43(7), 1356–1379. doi:10.1175/JPO-D-12-0164.1

Neumann, A. and Macintyre, I., 1985. Reef response to sea level rise: Keep-up, catch-up or give-up. *Proceedings of the Fifth International Coral Reef Congress*, Volume 3 (Tahiti), pp. 105–110.

Nicholls, R.J. and Cazenave, A., 2010. Sea-level rise and its impact on coastal zones. *Science*, 3289(5985), 1517–1520. doi:10.1126/science.1185782

Norcross, Z.M.; Fletcher, C.H., and Merri, M., 2002. Annual and interannual changes on a reef-fringed pocket beach: Kailua Bay, Hawaii. *Marine Geology*, 190(3–4), 553–580.

Parsons, T., 2021. The weight of cities: Urbanization effects on Earth's subsurface. *AGU Advances*, 2(1), e2020AV000277. doi:10.1029/2020AV000277

Perry, C.T.; Murphy, G.N.; Kench, P.S.; Smithers, S.G.; Edinger, E.N.; Steneck, R.S., and Mumby, P.J., 2013. Caribbean-wide decline in carbonate production threatens coral reef growth. *Nature Communications*, 4(1), 1402. doi:10.1038/ncomms2409

Pomeroy, A.; Lowe, R.; Symonds, G.; Van Dongeren, A., and Moore, C., 2012. The dynamics of infragravity wave transformation over a fringing reef. *Journal of Geophysical Research: Oceans*, 117(C11), C11022. doi:10.1029/2012JC008310

REVOSIMA (Volcanological and Seismological Monitoring Network of Mayotte), 2023. *Bulletin de l'activité sismo-volcanique à Mayotte*. https://www.ipgp.fr/actualites-du-revosima/

Risandi, J.; Hansen, J.E.; Lowe, R.J., and Rijnsdorp, D.P., 2020. Shoreline variability at a reef-fringed pocket beach. *Frontiers in Marine Science*, 7, 445. doi:10.3389/fmars.2020.00445

Rovere, A.; Stocchi, P., Vacchi, M., 2016. Eustatic and relative sea level changes. *Current Climate Change Reports*, 2, 221–231.

Samosorn, B. and Woodroffe, C., 2008. Nearshore wave environments around a sandy cay on a platform reef, Torres Strait, Australia. *Continental Shelf Research*, 28(16), 2257–2274.

Saunders, M.I.; Albert, S.; Roelfsema, C.M.; Leon, J.X.; Woodroffe, C. D.; Phinn, S.R., and Mumby, P.J., 2016. Tectonic subsidence provides insight into possible coral reef futures under rapid sea-level rise. *Coral Reefs*, 35, 155–167. doi:10.1007/s00338-015-1365-0

Sheppard, C.; Dixon, D.; Gourlay, M.; Sheppard, A., and Payet, R., 2005. Coral mortality increases wave energy reaching shores protected by reef flats: Examples from the Seychelles. *Estuarine, Coastal and Shelf Sciences*, 64(2–3), 223–234.

Shirzaei, M.; Freymueller, J.; Törnqvist, T.E.; Galloway, D.L.; Dura, T., and Minderhoud, P.S.J., 2021. Measuring, modelling and projecting coastal land subsidence. *Nature Reviews Earth and Environment*, 2(1), 40–58. doi:10.1038/s43017-020-00115-x

Storlazzi, C.D.; Elias, E.; Field, M.E., and Presto, M.K., 2011. Numerical modeling of the impact of sea-level rise on fringing coral reef hydrodynamics and sediment transport. *Coral Reefs*, 30(S1), 83–96. doi:10.1007/s00338-011-0723-9

Tzevahirtzian, A.; Zaragosi, S.; Bachèlery, P.; Biscara, L., and Marchès, E., 2020. Submarine morphology of the Comoros volcanic archipelago. *Marine Geology*, 432, 106383.

Upton, B.G.J., 1982. *Oceanic islands*. In: Nairn, A.E.M. and Stehli, F.G. (eds.), *The Ocean Basins and Margins*. New York: Springer, 776p.

Vittecoq, B.; Deparis, J.; Violette, S.; Jaouën, T., and Lacquement, F., 2014. Influence of successive phases of volcanic construction and erosion on Mayotte's Island's hydrogeological functioning as determined from a helicopter-borne resistivity survey correlated with borehole geological and permeability data. *Journal of Hydrology*, 509, 519–538. doi:10.1016/j.jhydrol.2013.11.062

Vousdoukas, M.I.; Velegrakis, A.F.; Dimou, K.; Zervakis, V., and Conley, D.C., 2009. Wave run-up observations in microtidal, sediment-starved pocket beaches of the Eastern Mediterranean. *Journal of Marine Systems*, 78, S37–S47. doi:10.1016/j.jmarsys.2009.01.009

Webster, J.M.; Braga, J.C.; Clague, D.A.; Gallup, C.; Hein, J.R.; Potts, D.C.; Renema, W.; Riding, R.; Riker-Coleman, K.; Silver, E., and Wallace, L.M., 2009. Coral reef evolution on rapidly subsiding margins. *Global and Planetary Change*, 66(1–2), 129–148. doi:10.1016/j.gloplacha.2008.07.010

Wu, A.L.; Wei, M., and D'Hondt, S., 2022. Subsidence in coastal cities throughout the world observed by InSAR. *Geophysical Research Letters*, 49(7), e2022GL098477.

Yates, M.L.; Le Cozannet, G.; Garcin, M.; Salaï, E., and Walker, P., 2013. Multidecadal atoll shoreline change on Manihi and Manuae, French Polynesia. *Journal of Coastal Research*, 29(4), 870–882. doi:10.2112/JCOASTRES-D-12-00129.1

Young, L.R., 1989. Wave transformation over coral reefs. *Journal of Geophysical Research: Oceans*, 94(C7), 9779–9789.